

Article

Effect of Cobalt Composition on Electrochemical Behavior of Platinum-Based Catalyst towards Hydrogen Evolution Reaction

Duc Thanh Nguyen, Hang Thi Thuy Nguyen, Hung Cam Ly and An Thi Xuan Duong *

Ho Chi Minh City University of Natural Resources and Environment (HCMUNRE), Ho Chi Minh City, 700000, Viet Nam

* Correspondence: cplab.hcmunre@gmail.com; Tel.: +84 2839914212

Received: Apr 8, 2022; Accepted: May 8, 2022; Published: Jun 30, 2022

Abstract: The hydrogen production from water electrolysis is of interest as a renewable energy generation technology. However, the high price of noble platinum (Pt) catalysts for the hydrogen evolution reaction (HER) is a big challenge to use it. Herein, we fabricate cost-effective CoPt bimetallic alloys and explore the effect of Co composition on the electrochemical behavior of such alloys, which has been rarely reported. A series of $\text{Co}_{1-x}\text{Pt}_x$ ($x = 0.25; 0.5; 0.75$) alloys are prepared via a room-temperature chemical reduction route without using any surfactants/stabilizers that exhibit a uniform distribution in small particle sizes (ca. 3 nm) on the carbon surface. In terms of the HER, the incorporation of a suitable Co proportion into the Pt lattices enhance significantly the HER performance in an acidic environment. For instance, the $\text{Co}_{0.5}\text{Pt}_{0.5}$ NPs/C catalyst displays a low onset potential (16.67 mV) and a small Tafel slope ($19.60 \text{ mV dec}^{-1}$), which is different from other $\text{Co}_{1-x}\text{Pt}_x$ catalysts and commercial C-supported Pt (NPs) catalyst. This research result not only supplies a facile strategy to synthesize alloys but also guides the choice of a suitable proportion of transition metal into Pt lattice for electrochemical reactions in green energy storage and conversion technologies.

Keywords: Binary alloys, Hydrogen evolution reaction, Electrocatalyst, Green energy

1. Introduction

The increasing energy demands and environmental pollution crisis necessitate the development of green energy sources, which has been of interest as a promising alternative tendency for the future [1]. Over the past decades, hydrogen production from water electrolysis has attracted researchers' attention as renewable and green energy conversion technology because of its merits of abundant water reserves and no emissions [2]. Unfortunately, the high price of noble platinum electrocatalysts, which is the most efficient HER catalyst, has been considered the biggest challenge for commercializing such energy-generation technologies. At this juncture, many efforts have been devoted to fabricating robust support [3–5], and binary alloys [6–8] to enhance the electrocatalytic performance and lower the Pt utilization. Among binary alloys, Pt-Co has been considered a potential HER catalyst owing to the synergistic and electronic effect of Co and Pt [9]. As an example, Wang et al. [9] fabricated PtCo-Co/TiM catalyst for the alkaline HER that exhibited the 46.5 mA cm^{-2} current density at a 70 mV overpotential, which was 1.8-times higher than Pt NPs/C.

Although many recent studies have reported on fabricating PtCo binary alloys with high HER catalytic performance, the effect of cobalt composition on electrochemical HER properties of such binary alloy is rarely demonstrated. In this work, we fabricate and explore the effect of cobalt composition on the electrochemical behaviors of CoPt alloys towards the acidic HER. A series of bimetallic $\text{Co}_{1-x}\text{Pt}_x$ ($x = 0.25; 0.5; 0.75$) alloys was synthesized by the room-temperature chemical reduction approach to exhibit a uniform distribution in a small particle size on the surface of carbon supports. In terms of the HER, $\text{Co}_{1-x}\text{Pt}_x$ bimetallic alloys with a suitable proportion of Co into Pt lattices (i.e., $\text{Co}_{0.25}\text{Pt}_{0.75}$ NPs/C and $\text{Co}_{0.5}\text{Pt}_{0.5}$ NPs/C catalyst) showed the enhanced HER performance compared to C-supported Pt (NPs) catalyst with the highest performance obtained on $\text{Co}_{0.5}\text{Pt}_{0.5}$ NPs/C catalyst (onset potential of 16.67 mV, overpotential 19.85 mV, and Tafel slope of $19.60 \text{ mV dec}^{-1}$). While increasing the Co: Pt ratio up to 0.75:0.25, a decrease in both activity and stability was observed. This phenomenon is interpreted as the modification of the electronic structure of Pt when the incorporation of a suitable Co proportion into Pt lattices results in a decrease of the antibonding state, thereby promoting the hydrogen adsorption/desorption ability of Pt surface, consequently, the improved HER performance.

2. Materials and Methods

All chemical agents were commercially purchased and used without further purification. The agents were $\text{H}_2\text{PtCl}_6 \cdot 6\text{H}_2\text{O}$

(~38% Pt, Sigma-Aldrich), $\text{CoCl}_2 \cdot 6\text{H}_2\text{O}$ (98%, Sigma-Aldrich), NaBH_4 (98%, Sigma-Aldrich), and ethylene glycol (99.8%, Sigma-Aldrich). In a typical experiment, $\text{Co}_{1-x}\text{Pt}_x$ NPs ($x = 0.25; 0.5; 0.75$) alloys were deposited on the surface of carbon support by a modified chemical reduction reaction at room temperature by using a mixture of NaBH_4 and EG [10,11]. Briefly, 0.05 M of H_2PtCl_6 and 0.05 M CoCl_2 were added to a mixture (0.5 mL EG and 25 mL distilled water) with the different Pt: Co atomic ratios. Afterward, 50 mg of carbon nanoparticles were added to the above solution, followed by adjusting the pH value to 11. Next, the suspension was ultrasonicated for 15 min to form a homogeneous suspension. Then, NaBH_4 was gradually dropped into the prepared mixture and stirred for 120 min to conduct the reduction reaction. Finally, the products were centrifuged and washed with purged water, followed by drying at 80 °C for further analysis.

The X-ray diffraction (XRD, D2 PHASER), transmission electron microscopy (TEM, JOEL-JEM 2100F), and energy dispersive X-ray analysis (EDX, JOEL-JSM 6500F) were used to analyze the structure, morphology and particle size, and elemental composition, respectively. Additionally, an AutoLab potentiostat/galvanostat (PGSTAT302N) workstation (Metrohm Co., Ltd. Switzerland) was connected with a three-electrode cell, including a working electrode (glassy carbon (GCE), 5 mm). A reference electrode ($\text{Ag}/\text{AgCl}/(\text{sat. KCl})$) and counter electrode (Pt wire) were used to evaluate the electrochemical properties of made catalysts. The catalyst ink was prepared according to the process in previous studies [6,12]. The electrochemical surface area (ECSA) was calculated based on the hydrogen adsorption/desorption region in cyclic voltammetry (CV) in nitrogen-saturated 0.5 M H_2SO_4 at a 50 mV s^{-1} scan rate. The HER performance of the investigated electrocatalysts was tested by linear sweep voltammetry (LSV) in an acidic electrolyte at a scan rate of 5 mVs^{-1} . The catalytic stability for the HER was recorded by an accelerated durability test (ADT). All potential was converted to a normal hydrogen electrode (NHE) scale.

3. Results and Discussion

The effect of Co composition on the formed structure of $\text{Co}_{1-x}\text{Pt}_x$ NPs/C binary alloys was investigated by the XRD. Figure 1(a) shows XRD patterns of the $\text{Co}_{0.25}\text{Pt}_{0.75}$ NPs/C, $\text{Co}_{0.5}\text{Pt}_{0.5}$ NPs/C, and $\text{Co}_{0.75}\text{Pt}_{0.25}$ NPs/C catalysts that exhibited typical diffraction peaks at 2θ degrees around 40°; 46°; and 70° of the (111); (200); and (220) facets of face-centered-cubic structure. Furthermore, the diffraction peak locations of $\text{Co}_{1-x}\text{Pt}_x$ NPs/C catalysts were laying between the standard fcc Pt (JCPDS 04-0802) and Co (JCPDS 15-0806), which was shifted to higher degrees than C-supported Pt (NPs) catalysts. This indicated the incorporation of Co atoms into Pt lattices (Fig. 1b). Additionally, the diffraction peaks were observed at 2θ degrees of ~25° of the (002) facet of carbon supports, suggesting the successful deposition of bimetallic $\text{Co}_{1-x}\text{Pt}_x$ alloys on the surface of the carbon support.

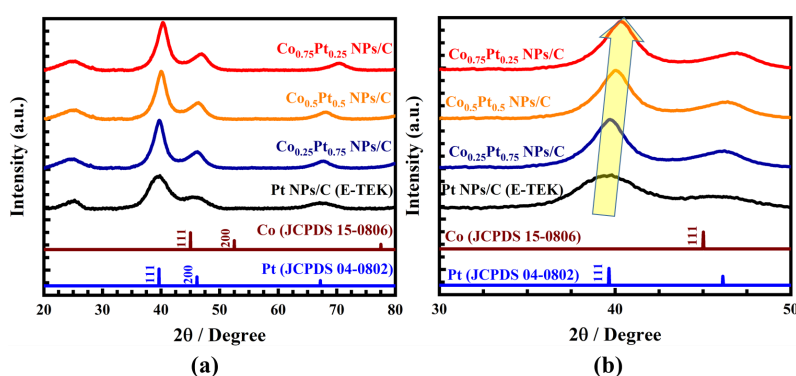


Fig. 1. (a) XRD patterns of series $\text{Co}_{1-x}\text{Pt}_x/\text{C}$ catalysts in 2θ ranges of (a) 20° – 80°; and (b) 20° – 50°.

Table 1. A summary of lattice parameters of a series $\text{Co}_{1-x}\text{Pt}_x$ NPs/C and commercial Pt NPs/C catalysts.

Catalysts	Diffraction peak location (°)			FWHM			Interplanar spacing (nm)			Coherent length (nm)		
	(111)	(200)	(220)	(111)	(200)	(220)	$d_{(111)}$	$d_{(200)}$	$d_{(220)}$	$D_{(111)}$	$D_{(200)}$	$D_{(220)}$
$\text{Co}_{0.75}\text{Pt}_{0.25}$ NPs/C	40.32	46.86	70.37	2.87	4.00	3.46	2.23	1.93	1.33	3.08	2.26	2.93
$\text{Co}_{0.5}\text{Pt}_{0.5}$ NPs/C	40.07	46.40	68.23	2.79	3.80	3.37	2.21	1.95	1.37	3.16	2.38	2.98
$\text{Co}_{0.25}\text{Pt}_{0.75}$ NPs/C	39.73	46.28	67.73	2.94	3.95	3.42	2.27	1.96	1.38	3.11	2.28	2.94
Co_0Pt_1 NPs/C	39.65	45.52	67.31	4.10	4.49	4.33	0.23	0.20	0.14	2.15	2.00	2.02

To further confirm the alloy formation, the interplanar spacing ($d_{(hkl)}$) and coherent length ($D_{(hkl)}$) of the obtained catalysts was calculated by Bragg's law and Debye-Scherrer's formula, respectively [13]. As listed in Table 1, the interplanar spacing ($d_{(hkl)}$) and coherent length ($D_{(hkl)}$) of bimetallic $\text{Co}_{1-x}\text{Pt}_x$ NPs/C catalysts exhibited a higher value than those of C-supported Pt (NPs)

electrocatalyst, showing the difference of atomic radius of Co (126 pm) and Pt (139 pm). These aforementioned results indicated the incorporation of Co into Pt lattices, leading to the formation of alloying Co with Pt.

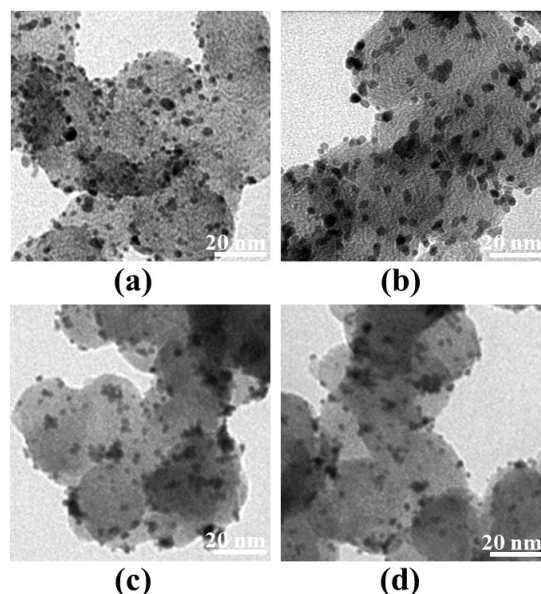


Fig. 2. TEM images of (a) Pt NPs/C; (b) $\text{Co}_{0.25}\text{Pt}_{0.75}$ NPs/C; (c) $\text{Co}_{0.5}\text{Pt}_{0.5}$ NPs/C; and (d) $\text{Co}_{0.75}\text{Pt}_{0.25}$ NPs/C catalysts.

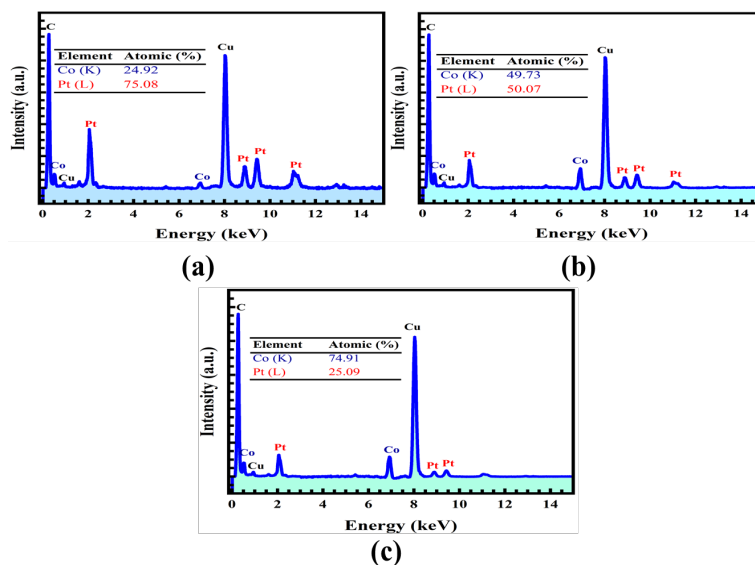


Fig. 3. EDX spectroscopy of (a) $\text{Co}_{0.25}\text{Pt}_{0.75}$ NPs/C; (b) $\text{Co}_{0.5}\text{Pt}_{0.5}$ NPs/C; and (c) $\text{Co}_{0.75}\text{Pt}_{0.25}$ NPs/C catalysts.

The morphology and particle size of the obtained catalysts were analyzed through transmission electron spectroscopy (TEM) images. Figure 2 demonstrates TEM images of different catalysts and indicates the spherical-like morphology with small particle size (ca. 3 nm), which agrees with the XRD results. TEM images also display the uniform distribution of $\text{Co}_{1-x}\text{Pt}_x$ binary alloys on the carbon support. These imply the enhanced performance of bimetallic $\text{Co}_{1-x}\text{Pt}_x$ NPs/C catalysts for the HER. In addition, EDX analysis was employed to record the elemental Co: Pt ratio in a series of the prepared catalysts. As shown in Fig. 3, the atomic composition of Co and Pt was 24.92:75.08 ($\text{Co}_{0.25}\text{Pt}_{0.75}$ NPs/C), 49.73:50.07 ($\text{Co}_{0.5}\text{Pt}_{0.5}$ NPs/C), and 74.91: 25.09 ($\text{Co}_{0.75}\text{Pt}_{0.25}$ NPs/C), which were approximate the theoretical atomic composition. These outcomes indicated that the modified chemical reduction process was a suitable method to fabricate the small particle-size $\text{Co}_{1-x}\text{Pt}_x$ binary alloys with a uniform distribution on the carbon surface.

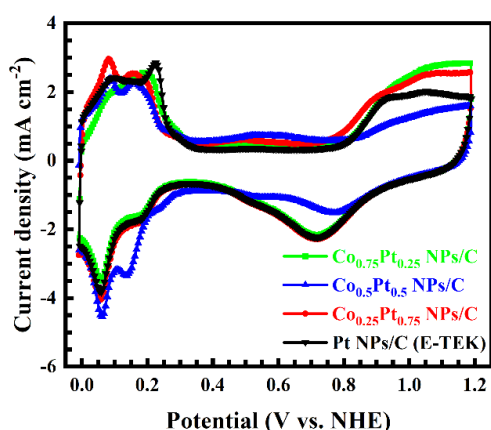


Fig. 4. Cyclic voltammetry (CV) curves of different catalysts in N_2 -saturated 0.5 M H_2SO_4 solution at 50 mV s^{-1} scan rate.

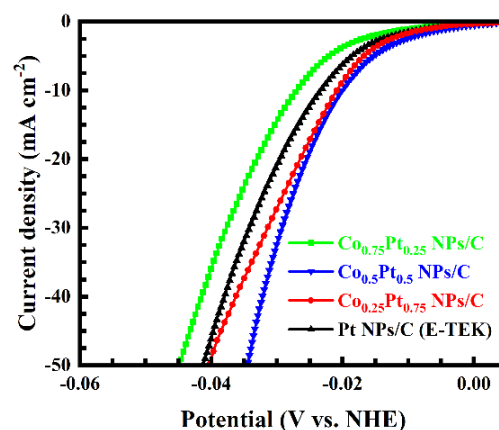


Fig. 5. Linear sweep voltammetry (LSV) curves of different catalysts in N_2 -saturated 0.5 M H_2SO_4 solution at a 5 mV s^{-1} scan rate.

The cyclic voltammetry (CV) test in an acidic electrolyte solution was carried out to investigate the effect of Co composition on the electrocatalytic performance of the made electrocatalysts. Figure 4 shows all CV curves of all catalysts in nitrogen-purged 0.5 M H_2SO_4 electrolyte at a 50 mV s^{-1} scan rate. The ECSA of $\text{Co}_{0.25}\text{Pt}_{0.75}$ NPs/C, $\text{Co}_{0.5}\text{Pt}_{0.5}$ NPs/C, $\text{Co}_{0.75}\text{Pt}_{0.25}$ NPs/C, and Pt NPs/C

(E-TEK) catalysts was calculated to be $78.45 \text{ m}^2 \text{ g}_{\text{Metal}}^{-1}$, $82.49 \text{ m}^2 \text{ g}_{\text{Metal}}^{-1}$, $80.14 \text{ m}^2 \text{ g}_{\text{Metal}}^{-1}$, and $70.25 \text{ m}^2 \text{ g}_{\text{Metal}}^{-1}$, respectively. This result indicates that the incorporation of Co into Pt lattices allowed more active sites and increased the contact area of the reactants on the catalyst surface. Besides, all the catalysts exhibited the current density in the H_2 adsorption region larger than the C-supported Pt (NPs) catalyst with the highest current density obtained on $\text{Co}_{0.5}\text{Pt}_{0.5}$ NPs/C catalyst, implying the enhanced hydrogen adsorption ability of $\text{Co}_{1-x}\text{Pt}_x$ NPs/C catalyst [14].

Furthermore, the HER performance of all $\text{Co}_{1-x}\text{Pt}_x$ NPs/C catalysts was examined in a nitrogen-purged $0.5 \text{ M H}_2\text{SO}_4$ electrolyte. As demonstrated in Fig. 5, the onset potential of $\text{Co}_{0.25}\text{Pt}_{0.75}$ NPs/C and $\text{Co}_{0.5}\text{Pt}_{0.5}$ NPs/C catalysts was 17.44 and 16.67 mV, respectively, which was shifted positively compared to commercial C-supported Pt (NPs) catalyst (20.70 mV). The onset potential of $\text{Co}_{0.75}\text{Pt}_{0.25}$ NPs/C catalyst was 24.54 mV. These results suggested that the HER on $\text{Co}_{1-x}\text{Pt}_x$ NPs/C catalysts with a proper cobalt composition was more easily made and worked faster than the commercial catalyst due to the synergistic effect of Co in binary alloys. In addition to onset potential, the overpotential at the current density at 10 mA cm^{-2} is usually used to evaluate the HER catalytic activity of electrocatalysts [15,16]. As a result, the overpotential of the $\text{Co}_{0.25}\text{Pt}_{0.75}$ NPs/C and $\text{Co}_{0.5}\text{Pt}_{0.5}$ NPs/C catalysts was 20.89 and 19.85 mV, respectively. These values had more positive shifts than the commercial catalyst (23.61 mV), whereas $\text{Co}_{0.75}\text{Pt}_{0.25}$ NPs/C catalysts exhibited a negative overpotential by 4.1 mV in comparison with the Pt NPs/C catalyst. This indicated the enhancement in the catalytic activity of $\text{Co}_{0.25}\text{Pt}_{0.75}$ NPs/C and $\text{Co}_{0.5}\text{Pt}_{0.5}$ NPs/C catalyst towards HER in an acidic environment versus the C-supported Pt (NPs) catalyst. Among $\text{Co}_{1-x}\text{Pt}_x$ NPs/C catalysts, the $\text{Co}_{0.5}\text{Pt}_{0.5}$ NPs/C catalyst exhibited the greatest onset potential and overpotential at 10 mA cm^{-2} current density, suggesting that such catalyst had best the HER activity.

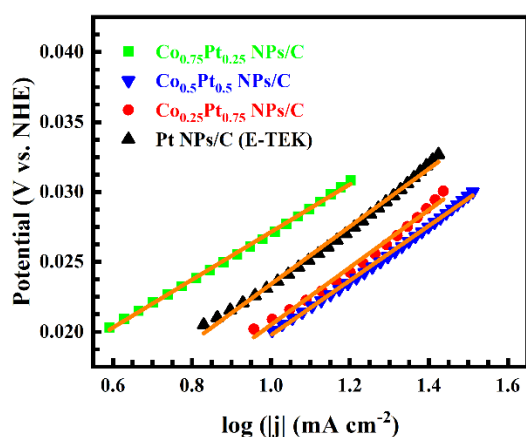


Fig. 6. The HER Tafel plots of catalysts in N_2 -saturated $0.5 \text{ M H}_2\text{SO}_4$ solution at a scan rate of 5 mV s^{-1} .

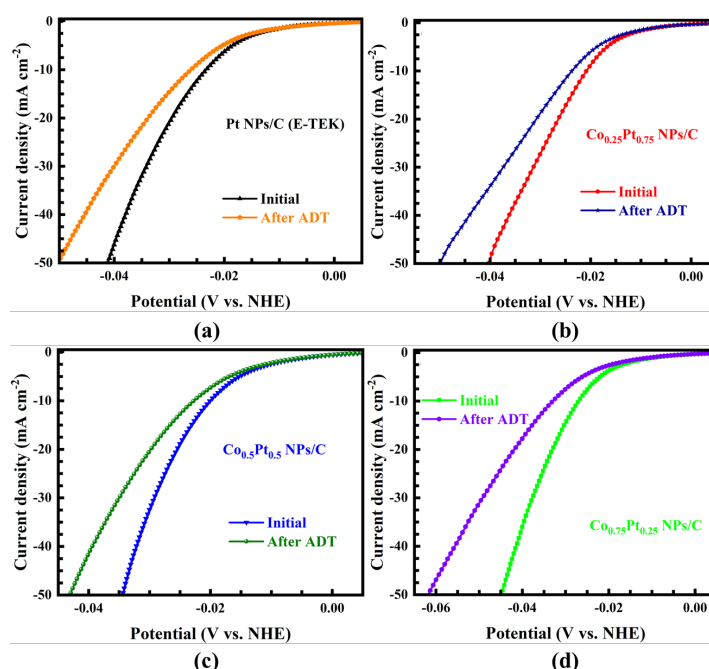


Fig. 7. Linear sweep voltammetry (LSV) curves of electrocatalysts before and after ADT in N_2 -saturated $0.5 \text{ M H}_2\text{SO}_4$ solution.

Table 2. Summary of the HER performance of bimetallic $\text{Co}_{1-x}\text{Pt}_x$ NPs/C catalysts in an acidic environment.

Catalysts	Onset potential mV_{NHE}	Overpotential at 10 mA cm^{-2} mV_{NHE}	Tafel slope mV dec^{-1}
$\text{Co}_{0.75}\text{Pt}_{0.25}$ NPs/C	24.54	27.71	20.61
$\text{Co}_{0.5}\text{Pt}_{0.5}$ NPs/C	16.67	19.85	19.60
$\text{Co}_{0.25}\text{Pt}_{0.75}$ NPs/C	17.44	20.89	20.50
Co_0Pt_1 NPs/C	20.70	23.61	20.39

The HER in acidic media is usually carried out according to three reaction routes including the Volmer reaction, the Heyrovsky reaction, and the Tafel reaction. To further confirm the reaction kinetic and conducted reaction pathway on the obtained HER

electrocatalysts, the Tafel slope was calculated based on the LSV curves of all HER catalysts. As depicted in Fig. 6, the Tafel slope of $\text{Co}_{0.25}\text{Pt}_{0.75}$ NPs/C, and $\text{Co}_{0.5}\text{Pt}_{0.5}$ NPs/C, and $\text{Co}_{0.75}\text{Pt}_{0.25}$ NPs/C catalysts was calculated to be 20.50, 19.60, and 20.61 mV dec^{-1} , respectively. These values are similar to the Tafel slope value of Pt NPs/C (20.39 mV dec^{-1}) under the same conditions as listed in Table 2, which suggests their preferable HER reaction kinetics [17]. Compared to the other HER catalysts, the prepared $\text{Co}_{0.5}\text{Pt}_{0.5}$ NPs/C catalyst had the smallest Tafel slope, indicating the remarkable enhancement in HER activity of the $\text{Co}_{0.5}\text{Pt}_{0.5}$ NPs/C electrocatalyst. Moreover, such Tafel slope values obtained on all HER electrocatalysts were nearby 30 mV dec^{-1} , showing that the reaction kinetics of all catalysts was confirmed via the Tafel steps and the HER was carried out based on the Volmer-Tafel mechanism.

In addition to the activity, catalytic stability was one of the factors to assess the performance of electrocatalysts in practical applications. Therefore, the accelerated durability test was conducted to record the long-term stability of $\text{Co}_{1-x}\text{Pt}_x$ NPs/C catalysts towards the HER. CV curves of the catalysts before and after 1000-cycling ADT in an acidic solution are shown in Fig. 7 and Table 3. As a result, the prepared $\text{Co}_{0.25}\text{Pt}_{0.75}$ NPs/C and $\text{Co}_{0.5}\text{Pt}_{0.5}$ NPs/C electrocatalysts showed high HER stability compared to the C-supported Pt (NPs) catalyst, while a reverse tendency was obtained for the $\text{Co}_{0.75}\text{Pt}_{0.25}$ NPs/C catalyst. The poor stability of the $\text{Co}_{0.75}\text{Pt}_{0.25}$ NPs/C catalyst was assigned to the dissolution of Co atoms in an acidic environment during the HER. These indicated that the appropriate incorporation of Co into Pt lattices could significantly enhance the HER stability of $\text{Co}_{1-x}\text{Pt}_x$ alloys.

Table 3. Summary of the HER performance of all investigated electrocatalysts before and after ADT.

Catalysts	Onset potential			Overpotential at 10 mA cm^{-2}		
	mV_{NHE}			mV_{NHE}		
	Before	After ADT	Degradation	Before	After ADT	Degradation
$\text{Co}_{0.75}\text{Pt}_{0.25}$ NPs/C	24.54	27.74	-3.20	27.71	33.19	-6.02
$\text{Co}_{0.5}\text{Pt}_{0.5}$ NPs/C	16.67	17.69	-1.02	19.85	22.72	-2.87
$\text{Co}_{0.25}\text{Pt}_{0.75}$ NPs/C	17.44	18.60	-1.16	20.89	23.12	-2.89
Co_0Pt_1 NPs/C	20.70	22.12	-1.42	23.61	28.43	-4.82

These experimental results indicated that $\text{Co}_{1-x}\text{Pt}_x$ binary alloys with the incorporation of a certain proportion of Co ($\text{Co}_{0.5}\text{Pt}_{0.5}$ NPs/C) were a promising electrocatalyst to improve the HER performance. The enhancement of $\text{Co}_{0.5}\text{Pt}_{0.5}$ NPs/C catalyst in this study can be explained due to (i) large ECSA, providing contact surface area for reactants on the prepared catalyst [18], and (ii) the incorporation of a suitable Co proportion into Pt lattices that modify the electronic structure of Pt, decreasing the antibonding state. Thereby, the H_2 adsorption/desorption ability is promoted on the Pt surface consequently by the improved HER activity [19].

4. Conclusions

In brevity, a series of $\text{Co}_{1-x}\text{Pt}_x$ binary alloys were fabricated through the modified chemical reduction process without using any surfactants or stabilizer agents at room temperature. The obtained $\text{Co}_{1-x}\text{Pt}_x$ NPs/C catalysts exhibited a small particle size (ca. 3 nm) with uniform distribution on the carbon support. Furthermore, the effect of Co composition on the structure and electrochemical behavior towards the HER of the prepared binary alloys was discussed. As a result, the $\text{Co}_{1-x}\text{Pt}_x$ NPs/C with the incorporation of the proper Co proportion ($\text{Co}_{0.25}\text{Pt}_{0.75}$ NPs/C and $\text{Co}_{0.5}\text{Pt}_{0.5}$ NPs/C) exhibited positive potential in both onset potential and overpotential at 10 mA cm^{-2} , indicating the enhanced HER performance versus the commercial catalyst. The $\text{Co}_{0.5}\text{Pt}_{0.5}$ NPs/C catalyst had the highest HER performance, while a reverse tendency was achieved on the $\text{Co}_{0.75}\text{Pt}_{0.25}$ NPs/C catalyst. This research result not only provides a facile route for fabricating binary alloys but also guides the choice of a suitable proportion of transition metal (such as Ni, Co, Fe, etc.) for Pt-M alloy for electrochemical reactions in green energy storage and conversion technologies.

Author Contributions: Duc Thanh Nguyen: Conceptualization, Investigation, Writing-Original draft preparation. Hang Thi Thuy Hang: Investigation, writing—review, and editing. Hung Cam Ly: Reviewing and Editing. An Thi Xuan Duong: Methodology, Data curation, Software, Reviewing and Editing.

Acknowledgments: The authors would like to thank you for the support of the Chemistry & Physics Laboratory, Ho Chi Minh City University of Natural Resources and Environment (HCMUNRE), Ho Chi Minh City, Viet Nam.

Conflicts of Interest: The authors declare no conflict of interest.

References

- Huynh, T.T.; Van Nguyen, A.; Pham, H.Q.; Vinh, N.H.; Bach, L.G. & Thanh Ho, V.T. One-Step Hydrothermal Synthesis of a New Nanostructure $\text{Ti}_{0.7}\text{Ir}_{0.3}\text{O}_2$ for Enhanced Electrical Conductivity: The Effect of pH on the Formation of Nanostructure, *J. Nanosci. Nanotechnol.*, **2018**, *18* 6928–6933.
- Guo, F.; Zou, Z.; Zhang, Z.; Zeng, T.; Tan, Y.; Chen, R.; Wu, W.; Cheng, N.; Sun, X. Confined sub-nanometer PtCo clusters as a highly efficient and robust electrocatalyst for the hydrogen evolution reaction, *J. Mater. Chem. A*, **2021**, *9*, 5468–5474.
- Pham, H.Q.; Huynh, T.T.; Van Nguyen, A.; Van Thuan, T.; Bach, L.G. & Van Ho, T.T. Advanced $\text{Ti}_{0.7}\text{W}_{0.3}\text{O}_2$ Nanoparticles Prepared via Solvothermal Process Using Titanium Tetrachloride and Tungsten Hexachloride as Precursors, *J. Nanosci. Nanotechnol.*, **2018**, *18*, 7177.
- Huynh, T.T.; Pham, H.Q.; Nguyen, A.V.; Nguyen, S.T.; Bach, L.G. & Ho, V.T.T. High Conductivity and Surface Area of Mesoporous $\text{Ti}_{0.7}\text{W}_{0.3}\text{O}_2$ Materials as Promising Catalyst Support for Pt in Proton-Exchange Membrane Fuel Cells, *J. Nanosci. Nanotechnol.*, **2019**, *19*, 877–881.
- Pham, H.Q.; Huynh, T.T.; Mai, A.T.N.; Ngo, T.M.; Bach, L.G. & Ho, V.T.T. Wire-like Pt on mesoporous $\text{Ti}_{0.7}\text{W}_{0.3}\text{O}_2$ Nanomaterial with Compelling Electro-Activity for Effective Alcohol Electro-Oxidation, *Sci. Rep.*, **2019**, *9*, 14791.
- Huynh, T.T.; Dang, N.N. & Pham, H.Q. Bimetallic PtIr nanoalloy on TiO_2 -based solid solution oxide with enhanced oxygen reduction and ethanol electro-oxidation performance in direct ethanol fuel cells, *Catal. Sci. Technol.*, **2021**, *11*, 1571–1579.
- Huang, T.-H.; Bhalothia, D.; Dai, S.; Yan, C.; Wang, K.-W.; Chen, T.-Y. Bifunctional Pt– SnO_x nanorods for enhanced oxygen reduction and hydrogen evolution reactions, *Sustain. Energy Fuels*, **2021**, *5*, 2960–2971.
- Pham, H.Q. & Huynh, T.T. Platinum–Copper Bimetallic Nanodendritic Electrocatalyst on a TiO_2 -Based Support for Methanol Oxidation in Alkaline Fuel Cells, *ACS Appl. Nano Mater.*, **2021**, *4*, 4983–4993.
- Wang, Z.; Ren, X.; Luo, Y.; Wang, L.; Cui, G.; Xie, F.; Wang, H.; Xie, Y. & Sun, X. An ultrafine platinum–cobalt alloy decorated cobalt nanowire array with superb activity toward alkaline hydrogen evolution, *Nanoscale*, **2018**, *10*, 12302–12307.
- Pham, H.Q.; Huynh, T.T.; Nguyen, A.V.; Mai, A.T.N.; Phan, V.T.T.; Bach, L.G.; Trinh, N.D. & Ho, V.T.T. Comparison the Rapid Microwave-Assisted Polyol Route and Modified Chemical Reduction Methods to Synthesize the Pt Nanoparticles on the $\text{Ti}_{0.7}\text{W}_{0.3}\text{O}_2$ Support, *Solid State Phenom.*, **2018**, *279*, 181–186.
- Huynh, T.T.; Pham, H.Q.; Van Nguyen, A.; V.T.T. Phan, A.T.N. Mai, T.D. Nguyen, D.-V.N. Vo, V.T.T. Ho, High conductivity of novel $\text{Ti}_{0.9}\text{Ir}_{0.1}\text{O}_2$ support for Pt as a promising catalyst for low-temperature fuel cell applications, *Int. J. Hydrog. Energy*, **2019**, *44*, 20944–20952.
- Pham, H.Q. & Huynh, T.T. Rutile $\text{Ti}_{0.9}\text{Ir}_{0.1}\text{O}_2$ -Supported Low Pt Loading: An Efficient Electrocatalyst for Ethanol Electrochemical Oxidation in Acidic Media, *Energy Technol.*, **2020**, *8*, 2000431.
- Pham, H.Q. & Huynh, T.T. Facile room-temperature fabrication of a silver–platinum nanocoral catalyst towards hydrogen evolution and methanol electro-oxidation, *Mater. Adv.*, **2022**, *3*, 1609–1616.
- Liu, Y.; Wang, Y.; Yang, P. & Gao, G. Composition adjustment of PtCoCu alloy assemblies towards improved hydrogen evolution and methanol oxidation reaction, *Int. J. Hydrog. Energy*, **2021**, *46*, 37311–37320.
- Chia, X.; Sutrisnoh, N.A.A. & Pumera, M.; Tunable Pt– MoS_x Hybrid Catalysts for Hydrogen Evolution, *ACS Appl. Mater. Interfaces*, **2018**, *10*, 8702–8711.
- Wei, M.; Huang, L.; Huang, S.; Chen, Z.; Lyu, D.; Zhang, X.; Wang, S.; Tian, Z.Q.; Shen, P.K. Highly efficient Pt-Co alloy hollow spheres with ultra-thin shells synthesized via Co-B-O complex as intermediates for hydrogen evolution reaction, *J. Catal.*, **2020**, *381*, 385.
- Zhang, X.-F.; Meng, H.-B.; Chen, H.-Y.; Feng, J.-J.; Fang, K.-M.; Wang, A.-J. Bimetallic PtCo alloyed nanodendritic assemblies as an advanced efficient and robust electrocatalyst for highly efficient hydrogen evolution and oxygen reduction, *J. Alloys Compd.*, **2019**, *786*, 232–239.
- Meng, H.-B.; Zhang, X.-F.; Pu, Y.-L.; Chen, X.-L.; Feng, J.-J.; Han, D.-M.; Wang, A.-J. One-pot solvothermal synthesis of reduced graphene oxide-supported uniform PtCo nanocrystals for efficient and robust electrocatalysis, *J. Colloid Interface Sci.*, **2019**, *543*, 17–24.
- Ren, W.; Zang, W.; Zhang, H.; Bian, J.; Chen, Z.; Guan, C. & Cheng, C. PtCo bimetallic nanoparticles encapsulated in N-doped carbon nanorod arrays for efficient electrocatalysis, *Carbon*, **2019**, *142*, 206–216.

Publisher's Note: IIKII stays neutral with regard to jurisdictional claims in published maps and institutional affiliations.

Copyright: © 2022 The Author(s). Published with license by IIKII, Singapore. This is an Open Access article distributed under the terms of the [Creative Commons Attribution License](https://creativecommons.org/licenses/by/4.0/) (CC BY), which permits unrestricted use, distribution, and reproduction in any medium, provided the original author and source are credited.